ACS OMEGA

http://pubs.acs.org/journal/acsodf

Article

N-Doped Carbon Dot Hydrogels from Brewing Waste for Photocatalytic Wastewater Treatment

Simone Cailotto,[⊥] Daniele Massari,[⊥] Matteo Gigli,* Carlotta Campalani, Massimo Bonini, Shujie You, Alberto Vomiero, Maurizio Selva, Alvise Perosa, and Claudia Crestini*

Cite This: *ACS Omega* 2022, 7, 4052−4061

Read Online

ACCESS | Metrics & More | Article Recommendations | Supporting Information

ABSTRACT: The brewery industry annually produces huge amounts of byproducts that represent an underutilized, yet valuable, source of biobased compounds. In this contribution, the two major beer wastes, that is, spent grains and spent yeasts, have been transformed into carbon dots (CDs) by a simple, scalable, and ecofriendly hydrothermal approach. The prepared CDs have been characterized from the chemical, morphological, and optical points of view, highlighting a high level of N-doping, because of the chemical composition of the starting material rich in proteins, photoluminescence emission centered at 420 nm, and lifetime in the range of 5.5−7.5 ns. With the aim of producing a reusable catalytic system for wastewater treatment, CDs have been entrapped into a polyvinyl alcohol matrix and tested for their dye removal ability. The results demonstrate that methylene blue can be efficiently adsorbed from water solutions into the composite hydrogel and subsequently fully degraded by UV irradiation.

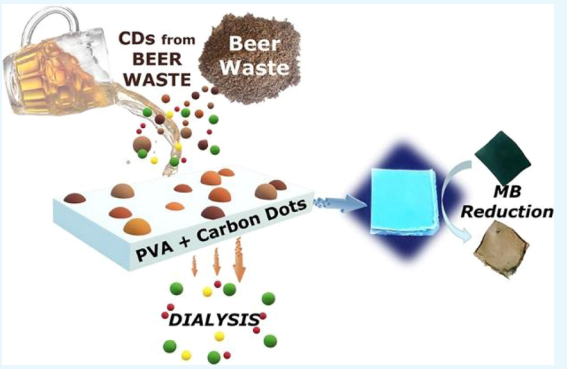

1. INTRODUCTION

The valorization of industrial wastes is one of the major targets for the transition toward a more sustainable and circular economy.[1] Different routes could be employed to fulfill this goal, from the generation of new platform chemicals or fuels to the formation of innovative high added-value materials.[2−5] In this respect, agro-industrial waste is of particular interest, among which that generated by the brewing industry represents an important fraction. Beer is indeed the fifth most diffused beverage in the world, with an average consumption of 23 liters/person per year.[6] During the beer production process, two major byproducts can be identified: beer spent grains (BSG) and beer spent yeasts (BSY) with an estimated annual production of 6×10^5 and 4×10^5 tons, respectively.[7,8] BSG are the solid waste obtained after the separation during the lautering step, and they are mainly constituted of a lignocellulosic material rich in fibers (hemicellulose and cellulose), lignin, proteins, and minerals.[9] On the other hand, BSY are recovered from the bottom of the fermenters and maturation tanks and usually still contain about 1.4%$_{wt}$ of residual beer.[10] The composition of this biomass is quite different from that of BSG, as it is richer in proteins and specifically shows a high content of glutamic acid.[11,12] On this basis, the upgrade of BSG and BSY wastes is of crucial importance to improve the sustainability of the beer production value chain. As of today, other than as the main constituent of vitamin-B-rich food spreads such as Marmite and Vegemite made from leftover brewers' yeast extract, the main use of these feedstocks is as a supplement in the animal diet, as it has been demonstrated that they can be effectively integrated into the diet of livestock, poultry, pigs, goats, and fish.[13,14] In the last few years, new strategies for the valorization of this underutilized biomass have been proposed, ranging from the production of second-generation fuels like bioethanol,[15,16] to the use as a fermentation substrate for the production of lactic acid,[17,18] succinic acid,[19] and proteins.[20] In addition, they have been employed for water treatment as adsorbent agents for heavy metals[21−23] and organic dyes.[24,25] However, the most important drawbacks limiting the full valorization of beer residues are the costs associated with the transportation of the biomass to the site of use and, above all, the need for a pretreatment step prior to any successive uses, because the high moisture and sugar content would lead to rapid decomposition.[26] An alternative way can be represented by the transformation into nanomaterials. In particular, in the last decade carbon dots (CDs) emerged as innovative materials.[27−29] CDs are classified as pseudospherical particles of diameter lower than 10 nm, usually showing a graphitic structure, complete solubility in water, and prominent

Received: September 29, 2021
Accepted: December 29, 2021
Published: January 28, 2022

photoluminescence (PL) properties.[30−32] In addition to these peculiar characteristics, the possibility to derive CDs from biomass employing easy and economic protocols makes them very appealing from a sustainability point of view.[33−35] Several studies have been recently carried out to understand their structure and PL behavior, highlighting a strict correlation with the adopted synthetic strategy.[36−38] In particular, hydrothermal treatments generally produce a mixture of organic fluorophores and CDs, both contributing to the final PL.[39,40] By isolating the two components, it has been shown that while CDs exhibit an excitation-dependent PL, the PL of the organic fluorophores is independent of the excitation wavelength.[41−43]

To date, the PL mechanism of CDs is still unclear. Numerous studies have been performed to unveil this mechanism, and three main hypotheses have come out, that is, quantum confinement, molecular state, and surface state, with the last one being the most accepted theory.[44]

CDs have been successfully tested for several applications such as energy capacitors,[45] biosensors,[46] photovoltaic[47] luminescent concentrators[48] and drug delivery materials.[49] The light-harvesting properties of CDs can also be exploited for photocatalytic reactions.[50−55] Because of their very peculiar chemical composition, beer residues may represent an ideal raw material to prepare CDs (Scheme 1). Nevertheless, the

Scheme 1. Valorization of Brewery Waste

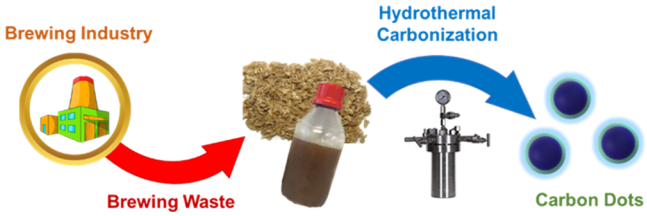

generation of CDs from this substrate has been only seldom investigated. To the best of our knowledge, the only available report deals with the preparation of CDs from BSG by hydrothermal treatment and their testing as a bioprobe for imaging.[56] Therefore, this represents the first comprehensive work on the valorization of brewing waste for the production of CDs, especially as regards the transformation of BSY. This brewing waste, rich in proteins, generates CDs with an intrinsically high level of N-doping.

In this work, we have converted the beer production wastes of two different beer styles (IPA and Stout) into CDs by hydrothermal carbonization (HTC) (Scheme 1). BSG and BSY were treated separately or blended to better simulate a large-scale adoption of the protocol, where all the residues would be more reasonably combined before any further transformation steps. The obtained CDs were characterized from the structural and optical points of view and then tested for their ability to catalyze the degradation reaction of a common dye. For this purpose, CDs were immobilized into a polyvinyl alcohol (PVA) hydrogel allowing for an easy recovery and recycling of the catalytic system. Last, but not least, we have demonstrated that this strategy permits avoiding costly and time-consuming dialysis treatments to separate the CDs from the organic fluorophores formed in the process, as the PVA matrix can itself play the role of a dialysis material.

2. RESULTS AND DISCUSSION

A set of different CDs were prepared by HTC for 24 h at 200 °C (see the Experimental Section for more details) following the same reaction protocol, while varying the organic precursors.[35] The treatment of BSG in MilliQ water produced grain IPA crude CDs (GI_c, 20%$_{wt}$ yield) and grain Stout crude CDs (GS_c, 14%$_{wt}$ yield). On the other hand, BSY were carbonized using the corresponding residual beer as a solvent, giving yeast IPA crude CDs (YI_c, 36%$_{wt}$ yield) and yeast Stout crude CDs (YS_c, 37%$_{wt}$ yield). Finally, a third set of samples was prepared from a 50:50 (w/w) mixture of BSG and BSY in the presence of the corresponding residual beer, generating grain yeast IPA crude CDs (GYI_c, 25%$_{wt}$ yield) and grain yeast Stout crude CDs (GYS_c, 26%$_{wt}$ yield). The reported yields are clearly affected by the nature of the substrates. While BSY are mainly composed of organic molecules, like proteins, and can thus easily undergo dehydration and decarboxylation reactions, BSG are a more recalcitrant substrate, because of the high content of carbohydrates and lignin that mainly result in sugars after the hydrothermal treatment.[13] The chemical composition of the precursors and the CDs was evaluated by CHNS analysis (Table 1).

Table 1. CHNS Results of the Raw Materials and of the Crude CDs (I: IPA Style and S: Stout Style)

sample	C [%]	H [%]	N [%]	N/C
BSGI	48.5 ± 0.2	7.0 ± 0.2	3.9 ± 0.1	0.08 ± 0.01
BSGS	45.5 ± 0.2	6.7 ± 0.1	3.3 ± 0.1	0.07 ± 0.01
BSYI	44.2 ± 0.2	6.5 ± 0.1	6.8 ± 0.1	0.15 ± 0.01
BSYS	42.3 ± 0.5	6.6 ± 0.2	6.9 ± 0.3	0.16 ± 0.01
GI_c	43.5 ± 0.3	5.7 ± 0.1	6.7 ± 0.1	0.15 ± 0.01
GS_c	43.9 ± 0.2	6.4 ± 0.4	6.8 ± 0.1	0.16 ± 0.01
YI_c	42.1 ± 0.8	7.0 ± 0.1	9.4 ± 0.2	0.22 ± 0.01
YS_c	39.9 ± 0.9	6.7 ± 0.3	9.0 ± 0.5	0.23 ± 0.01
GYI_c	41.0 ± 1	7.1 ± 0.1	8.6 ± 0.2	0.21 ± 0.01
GYS_c	41.4 ± 0.4	7.1 ± 0.1	8.1 ± 0.1	0.20 ± 0.01

The N/C ratio confirms that the nitrogen content of BSG is much lower than that of BSY, as the major fraction of components is solubilized in the wort during the beer production process, leading to a low amount of residual proteins. Generally, an increase of the N/C ratio can be observed in the CDs with respect to the starting materials. This result can be explained based on the mild reaction conditions of the HTC process, which cause thermal decomposition of the amino acids resulting in the formation of condensed heterocyclic structures with peptide bonds, in turn leading to a loss of H_2O rather than gaseous NH_3.[57] On the other hand, carbonization and decarboxylation reactions are responsible for the decrease of the carbon content in the CDs. The optical properties of the crude CDs were then investigated through UV−Vis and PL-PLE measurements (Figure 1).

Three broad absorption peaks centered at 250, 270, and 320 nm, with a long tail extended into the visible region, could be observed in all the samples. The peaks located in the lower wavelength region, that is, at 250 and 270 nm, can be respectively attributed to the $\pi-\pi^*$ transition of the C=C conjugated system and to the C=O $n-\pi^*$ transition, while the additional peak at 320 nm can be ascribed to the $\pi-\pi^*$ transition from nonbonding orbitals.[58] The PL/PLE spectra were registered at different excitation wavelengths (240−380 nm). The emission was found to be excitation-dependent,

https://doi.org/10.1021/acsomega.1c05403
ACS Omega 2022, 7, 4052−4061

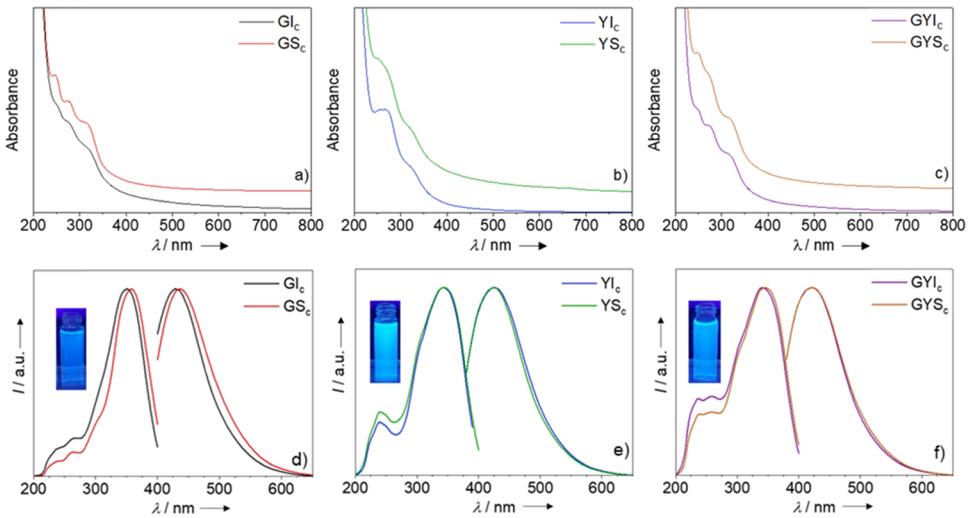

Figure 1. UV−Vis spectra of the synthesized CDs (a−c) and their normalized PL and PLE spectra recorded at an excitation wavelength of 350 nm (d−f).

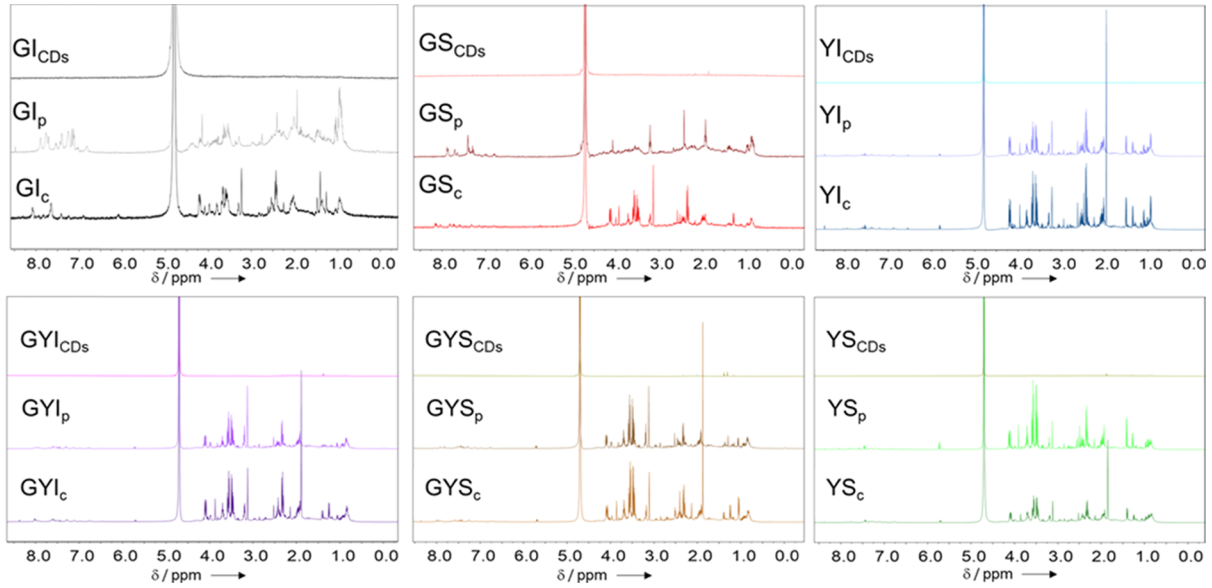

Figure 2. ^{1}H NMR spectra comparison of the crude CDs with the corresponding retentate and permeate fractions.

exhibiting a red shift as the excitation wavelength increased (Figure S1). All samples exhibit a bright blue emission with the maximum centered in the range of 420−440 nm, with a maximum excitation in the range of 340−350 nm.

The surface chemical groups of the crude CDs and of the precursors were investigated by Fourier transform infrared (FT-IR) spectroscopy (Figure S2). Similar peaks can be identified in all the starting materials regardless of their origin. The same considerations could also be applied to the CD samples, which highlighted a very similar composition. A typical broad peak, due to the stretching vibration band of O−H and N−H that covers the entire region from 3100 to 3700 cm^{-1}, can be noticed. After the HTC treatment, more evident peaks were formed at 1650 and 1570 cm^{-1}, respectively, caused by the stretching of carbonyl groups and the synergistic contribution of the bending of N−H and the stretching of C=C, because of the formation of the carbogenic core. These data are in agreement with the results of the CHNS analysis, where an increase of the nitrogen content was observed after the reaction. To evaluate the presence of organic molecules that could affect the PL behavior of the CDs, the samples were analyzed through ^{1}H NMR. As is visible in Figure 2, all the samples present several peaks, especially in the aliphatic region, suggesting the presence of organic molecules in the final product.

A diffusion order-nuclear magnetic resonance (DOSY-NMR) experiment allowed for an estimation of the MWs of these compounds, which is in the range of 150−300 Da (Figure S3 and Table S1). To purify the CDs, the extraction of the organic molecules from the crude samples was achieved by dialysis in MilliQ water. Both the permeate fraction (XX$_p$), containing the organic molecules, and the retentate fraction (XX$_{CDs}$), consisting of pure CDs, were collected by solvent evaporation. The success of the purification step was confirmed by the ^{1}H NMR analysis of the two fractions. As shown in Figure 2, the retentate fractions showed a silent spectrum, which confirms the presence of the solely carbonaceous core,

https://doi.org/10.1021/acsomega.1c05403
ACS Omega 2022, 7, 4052−4061

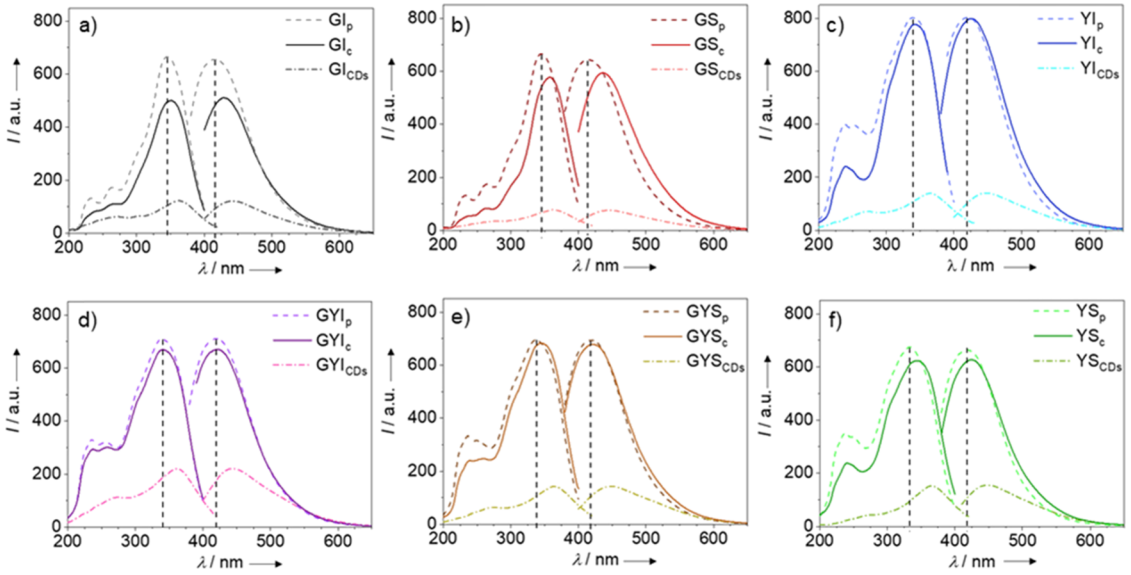

Figure 3. Maximum of PL and PLE of the crude CDs compared with their retentate and permeate fractions ((a) from spent grain IPA, (b) from spent grain Stout, (c) from spent yeast IPA, (d) from mixed spent grain and yeast IPA, (e) from mixed spent grain and yeast Stout, and (f) from spent yeast Stout).

while the spectra of the permeate fractions fully resembled those of the crude CDs.

The morphology and size of the purified CDs (hereinafter simply called CDs) were respectively investigated by scanning electron microscopy (SEM) and laser diffraction analysis (LDA), revealing a graphitic material composed of particles with an average dimension of about 100 nm (Figure S4). FT-IR analysis (Figure S5) revealed that, compared to crude samples, CDs display similar bands, although a marked reduction of the peaks associated with the C═O stretching and N−H bending, which could be attributed to the organic molecules, was observed. As already reported in the literature,[41,59] the dialysis procedure affected the optical properties of the materials, higher in the crude samples because of the presence of fluorophores. PL and PLE spectra of the two fractions (permeate and CDs) and of the crude CDs are reported in Figure 3.

By analyzing the curves, it emerges that the luminescence properties of the crude samples are the sum of two distinct contributions, the first of lower intensity, due to the carbogenic core, and the second, much stronger, associated with the fluorophore compounds. Similar results have been described in a previous study that demonstrated the synergistic contribution of the organic fluorophores and the carbon core in defining the luminescence characteristics of CDs.[43] The PL emission still maintains a dependence on the excitation wavelength characterized by the typical red shift (see, for instance, Figure S1) and the decrease of the maximum of the emission upon changing of the excitation wavelength. The wavelength-dependent response is a phenomenon widely observed in purified CDs and is caused by the different surface states near to the Fermi level.[60] On the contrary, according to the Kasha−Vavilov rules, the emission spectrum of a pure fluorophore molecule is independent of the excitation wavelength.[61] Therefore, the wavelength-dependent emission of the permeate samples is further evidence of the presence of a plurality of molecules. The observed differences are particularly evident from comparing the quantum yield (QY) of the two fractions (Table 2).

Table 2. QYs and Lifetimes (τ) of the Permeate and Retentate Fractions of CDs Calculated at 316 and 372 nm

samples	QY_{340nm} [%]	τ_{316nm} [ns]	τ_{372nm} [ns]
GS_p	6.8	7.52	6.07
GS_{CDs}	1.4	6.54	4.73
GI_p	6.0	7.91	5.99
GI_{CDs}	2.2	7.21	5.70
YI_p	10.5	8.44	7.68
YI_{CDs}	2.3	7.07	5.38
YS_p	12.9	8.60	7.42
YS_{CDs}	1.9	6.65	5.30
GYI_p	10.4	7.92	7.05
GYI_{CDs}	2.0	6.41	2.50
GYS_p	11.3	8.66	7.28
GYS_{CDs}	2.1	6.71	4.88

All the permeate materials exhibit a higher QY than the corresponding CDs, once again confirming the formation of fluorophores during the HTC treatment. In general, CDs have an average QY of 2%, while values in the range of 10−13% are calculated for the permeate fractions. Other literature studies describe QY for nondialyzed CDs of about 15−20%,[33] in agreement with the values here reported for the permeate fraction. On the other hand, the QYs of dialyzed CDs obtained from biomass generally do not exceed 7−8% and are usually lower compared to those obtained from pure molecules.[62,63]

Despite this difference, the average lifetime (τ) at 316 nm of the two fractions is very similar, because the τ of the CDs are only slightly shorter compared to those of the fluorophores. Enhanced differences were revealed at 372 nm, as the τ values of CDs are much shorter compared to those of the corresponding permeate fractions, thus confirming the separation of the different components involved in the PL behavior of the crude samples thanks to the dialysis treatment, as already documented by the PL spectra (Figure S1). The here reported values are supported by the study of Schneider et al.,[43] which described the fluorescence behavior of citric acid-derived CDs. The authors highlighted that the fluorescence

https://doi.org/10.1021/acsomega.1c05403
ACS Omega 2022, 7, 4052−4061

arising from pure citrazinic acid (the most common fluorophore in citric acid-derived CDs) possesses an average lifetime around 7 ns, while purified CDs showed a reduced lifetime fluorescence behavior, with an average τ of 5−6 ns.

The results here presented demonstrate that no significant differences in the final characteristics of the CDs have been achieved by varying the beer waste used for their synthesis. On these bases, the blending approach was considered the most promising, as it better simulates an industrial setup (i.e., where all wastes would be preferentially mixed before treatment), and the relative samples have been therefore chosen for further investigation.

A possible application of the prepared CDs is as catalysts for the photodegradation of dyes, such as methylene blue (MB). This last is a pollutant commonly found in the wastewater of industrial sites,[64] especially textile industries, and its removal by simple and affordable methods is of crucial interest. The CD-assisted photodegradation of MB has been already assessed both under sunlight and UV irradiation.[65,66] In particular, Josuf et al. reported a complete conversion of a 1 ppm solution of MB under solar light after 10 h of simulated solar irradiation employing CDs obtained from eggshell membrane ashes.[67] To confirm the ability of the brewing waste-based CDs to catalyze this reaction, a 2 g/L water solution of CDs containing 5 ppm of MB was irradiated under UV light (365 nm). Both crude specimens and CDs (GYS_c and GYS_{CDs}, respectively) were tested, and the results have been compared with a negative control. The GYS_{CDs} sample shows higher catalytic activity than GYS_c, as a complete degradation of the MB was achieved in 24 h, with an increase of 63% (Figure 4) with respect to the control (Figure S6a), while

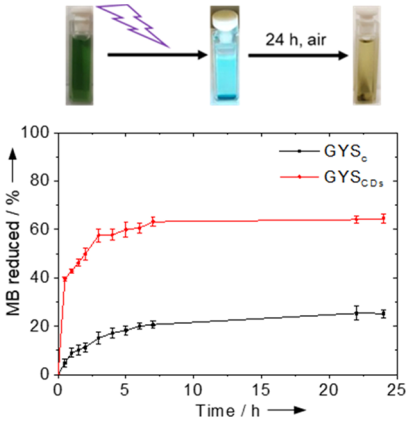

Figure 4. Kinetics of MB degradation by GYS_c and GYS_{CDs}.

GYS_c showed an enhancement of only 25% (Figure 4). As reported in the literature, the photocatalytic mechanism of degradation of MB with CDs occurs via the generation of an excited electron from the UV-irradiated CDs that are then involved in a two-electron-step photoreduction of MB leading to the colorless leuco MB.[68] The calculated photodegradation constants for both dialyzed and crude CDs (3×10^{-3} vs 8×10^{-4} min^{-1}) give a clear indication of the higher performances of the dialyzed CDs (Figure S6b).

This suggests that the presence of organic fluorophores not only affects the PL of CDs, as already demonstrated in the literature,[43] but also negatively influences their photocatalytic activity, supporting the need for a purification step to allow for an accurate evaluation of the photocatalytic behavior of the CDs and to achieve better performances. As reported in the literature for other photocatalytic systems,[69] the decrease in photodegradation activity could be ascribed to the presence of fluorophore molecules on the surface of CDs, which decreases the relative amount of active sites available for the adsorption of MB.

To gain further insight into the mechanism of photocatalytic degradation, further tests were carried out. The photocatalytic activity of CDs was investigated in the presence of isopropyl alcohol as a hydroxyl radical scavenger. The results obtained (data not shown) indicate no influence of this scavenger on the photocatalytic activity, as a complete degradation of the MB was observed in 24 h, meaning that the hydroxyl radical plays a minor role in the photodegradation mechanism. Similar results were obtained by performing the reaction under inert conditions removing the dissolved oxygen, suggesting that also the dissolved O_2 and the superoxide radicals that could be formed do not affect the reaction.

Because the immobilization of CDs on a support would facilitate the handling of the catalytic system, avoid leaching issues, and permit multiple working cycles, thus moving one step further toward large-scale adoption of the technology, the embedding of the CDs in a polymeric matrix was considered. In this respect, previous studies showed that the generation of CD-loaded composites based on PVA enhances both the mechanical properties of the hydrogels and the PL of the CDs.[56,70,71] These materials have been employed for sensing of food colorants and absorption of dyes.[72,73] On the other hand, the use of purified CDs integrated into polymeric matrices for the photodegradation of dyes has been only described by Nayak et al.[74] The authors demonstrated that a CD-containing polyvinylpyrrolidone hydrogel displays a promising response toward the degradation of crystal violet and malachite green.

More importantly, the use of the PVA hydrogel serves a dual scope. On the one hand, it can act as a reusable catalytic platform where to entrap the CDs, absorb the MB, and let the degradation reaction occur under UV irradiation. On the other hand, it can be used as a "dialysis membrane" for the separation of the carbonaceous particles from the fluorophore molecules. For this purpose, two CD-PVA hydrogels were prepared, each containing a different concentration of crude CDs (GYS_c): 8 wt % (w_{CDs}/w_{PVA}, PVA8) and 4 wt % (w_{CDs}/w_{PVA}, PVA4). Samples were prepared from a 10%$_{wt}$ solution of PVA in water, mixed with a solution of CDs (0.02 g/mL), and stirred at 45 °C for 0.5 h and then at 95 °C for 2 h followed by several freeze/thaw cycles (see the Experimental Section for more details).[75] The resulting hydrogel showed a light brown color under the daylight and a homogeneous blue fluorescence under UV light (Figure 5a).

A release test, to evaluate the kinetics of washout of the fluorophores from the hydrogel matrix, was performed. The process was carried out in water, and the amount of released material was determined by measuring the absorbance of the solution over time. After 3 days of incubation, a plateau corresponding to the release of about 90% of the entrapped materials was reached for both samples (Figure S7).

After the treatment and a further washing step with water, the hydrogels retain more than 70% of the initial fluorescence (Figure 5b and Figure S8), indicating that the CDs are still trapped in the polymer matrix, thanks to the strong hydrogen bonding interactions between the polymer chains and various functional groups present on the CDs surface,[73] while the fluorophores have been released. This procedure demonstrates

https://doi.org/10.1021/acsomega.1c05403
ACS Omega 2022, 7, 4052−4061

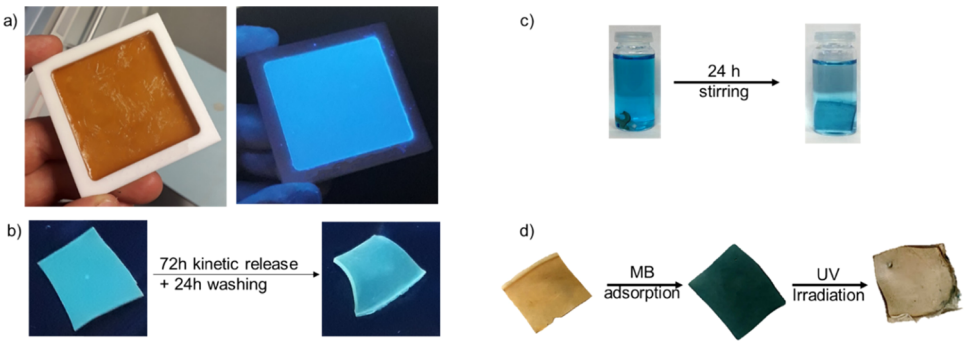

Figure 5. (a) PVA-CD hydrogel under visible light and UV light, (b) PVA-CD hydrogel fluorescence before and after washing treatment, (c) MB absorption test on PVA4 hydrogel, and (d) PVA4 hydrogel before and after MB absorption and after 24 h of UV irradiation.

for the first time that the PVA matrix can be efficiently utilized as a "dialysis membrane" to purify the CDs from the organic fluorophores and allows, in view of a potential scale up, to directly use the material coming from the HTC treatment, without the need for time- and resource-consuming purification steps.

Subsequently, the MB adsorption capability of PVA4 and PVA8 (after the treatment) was studied. By immersion for 24 h in a 5 ppm MB solution, the hydrogels turned dark blue (Figure 5c), confirming the successful adsorption of the dye. UV−Vis analysis of the remaining solution permitted to quantitatively determine the amount of MB absorbed, respectively, equal to 60 and 31% for PVA4 and PVA8. These results can be explained taking into consideration that the higher concentration of CDs, that act as a crosslinking agent, limits the swelling of the PVA8 hydrogel, thus resulting in a lower amount of soaked MB.[74,76]

Finally, the MB-containing hydrogels were irradiated under UV light at 365 nm, and the degradation of the dye was qualitatively evaluated visually. Indeed, as reported in Figure 5d, after 24 h of irradiation, the color of the hydrogels turned brown, indicating that an effective degradation occurred. The reusability of the PVA-CD matrix was evaluated by performing five cycles of adsorption and photodegradation of MB. As shown in Figure S9, after the fifth cycle the photocatalytic activity was fully retained, demonstrating the efficacy of the heterogeneous catalytic system for repeated photodegradation of pollutant dyes, that is, significant leaching of CDs during repeated use of the composite hydrogel could be excluded.

3. CONCLUSIONS

In this contribution, an easy, scalable, and cost-effective strategy for the upgrade of one of the most abundant byproducts of the agri-food value chain into an immobilized catalytic system has been proposed. In particular, beer waste (BSG and BSY) has been transformed into CDs by hydrothermal treatment. The nanomaterials, which show an intrinsically high degree of N-doping due to the peculiar chemical composition of the precursors, display PL emission properties centered at 420 nm. Because organic fluorophores are also formed during the process, CDs have been successfully purified by dialysis, leading to the isolation of carbonaceous particles with an average dimension of 100 nm, which tend to arrange into aggregates after drying. The generated CDs were tested with promising results in the photocatalytic degradation of MB, with the purified materials highlighting superior performances with respect to the crude samples.

With the aim of implementing this strategy into a more efficient technological tool, a CD-containing composite hydrogel was fabricated. The employment of a PVA-based polymeric matrix permitted not only to efficiently entrap the CDs, allowing for an easy recovery of the catalytic system after use, but also to avoid the dialysis step for CD purification, as the organic molecules were simply removed from the hydrogel by preliminary washing with water. Efficient soaking of MB from a water solution by the composite hydrogel and subsequent complete degradation of the dye after 24 h of irradiation with UV light demonstrated the effectiveness of the proposed solution.

Overall, these results can pave the way toward the development of innovative wastewater treatments for dye removal based on nanomaterials deriving from natural waste resources. In this framework, also the brewing industry would significantly benefit from the valorization of the byproducts, leading to the creation of more sustainable and circular economy pathways.

4. EXPERIMENTAL SECTION

4.1. Reagents. BSGS, BSYS, BSGI, and BSYI, where S and I stand for Stout and IPA, respectively, were kindly supplied by two locally operating microbreweries (B.A.V. s.r.l. and D.B.C. s.r.l.). Absolute ethanol, deuterium oxide, potassium bromide (KBr), PVA, and MB were analytical-grade reagents purchased from Sigma-Aldrich and were used as received. Milli-Q purified water was used in all the experiments unless otherwise stated.

4.2. Pretreatment of the Raw Materials. BSG were centrifuged at 15,000 rpm to remove water, and the solid residue was air-dried to constant weight. BSY were centrifuged to separate the residual beer and the solid fraction. The final product was air-dried to constant weight. Dry BSG and BSY were ground to fine powders.

4.3. CD Synthesis. CDs were prepared by HTC treatment. In more detail, a mixture composed of the biomass (either single waste or 1:1 w/w mixture of BSG and BSY of the same beer style) and the solvent (water or residual beer) in a 1:5 w/w ratio was let to react in an autoclave at 200 °C for 24 h under autogenous pressure. The reaction mixture was then filtered to collect the liquid fraction containing both CDs and organic fluorophores (crude CDs). CD purification was carried out in MilliQ water for 7 days using dialysis cassettes (Slide-A-Lyzer dialysis cassette) with a molecular weight cutoff of 2 kDa. Finally, the dialyzed solution was freeze-dried to yield purified CDs.

https://doi.org/10.1021/acsomega.1c05403
ACS Omega 2022, 7, 4052−4061

4.4. CD Characterization. A ZEISS ΣIGMA field emission scanning electron microscope was used to record images of the CDs. Samples were deposited on silicon wafers and analyzed in their pristine state (i.e., without any coating) at an accelerating voltage of 3 kV with an In-Lens secondary electron detector. LDA was performed on a Malvern Mastersizer 3000 equipped with a Hydro EV wet dispersion unit, including an in-line sonication probe for agglomerate dispersion. The chemical composition of the raw materials and of the produced CDs was evaluated by CHNS analysis by means of an Elementar UNICUBE instrument. All analyses have been carried out at least in triplicate, and the reported results represent the average ± standard deviation. The UV−Vis spectra were acquired in Milli-Q aqueous solutions with an Agilent 8456 spectrophotometer in the range of 800−200 nm. PL and PLE spectra were obtained with a PerkinElmer LS 55 fluorescence spectrophotometer in the range of 650−200 nm. For both techniques, if not otherwise stated, the solution concentration was 0.125 mg/mL. QY and fluorescence lifetime (τ) were determined by means of a FLS980 photoluminescence spectrometer from Edinburgh Instruments. For QY measurement, an integrating sphere assembly, accessory to the FLS980 spectrometer, was used to collect the emission. Samples were excited by 340 nm monochromatic light from a Xe lamp. For lifetime analysis, measurements were performed by exciting the samples with two different sources, a picosecond pulsed LED (EPLED-320, λ = 315.8 nm, pulse width: 940.4 ps, bandwidth: 9.8 nm) and a picosecond pulsed diode laser (EPL-375, λ = 371.8 nm, pulse width: 64.0 ps), and the emission was studied at 420 nm. FT-IR spectra were recorded from potassium bromide (KBr) discs, in a spectral range of 4000−400 cm^{-1} using a PerkinElmer Spectrum One spectrophotometer. ^{1}H and ^{13}C NMR spectra were collected on a Bruker Magnet System spectrometer 400′54 Ascend (^{1}H: 400 MHz; ^{13}C: 100.6 MHz).

4.5. PVA-CD Hydrogel Preparation. CD-containing PVA hydrogels were prepared by freezing/thawing following a previously reported procedure with minor modifications.[76] Briefly, a 10%$_{wt}$ solution of PVA in water was mixed with a solution of CDs (0.02 g/mL) and stirred at 45 °C for 0.5 h and then at 95 °C for 2 h to promote the full dissolution of PVA. The homogeneous PVA/CD solution was subsequently cast into PTFE mold and subjected to seven freezing−thawing cycles. Two PVA-CD hydrogels, PVA4 and PVA8, respectively containing 4 and 8%$_{wt}$ CDs (with respect to the PVA content) were prepared.

4.6. Release of Crude CDs from the PVA Hydrogel. The crude CD-loaded PVA hydrogel (20 × 20 mm, 80 mg ca.) was incubated in 30 mL of water and stirred for 72 h at 150 rpm and 25 °C in an ARGOlab shaker incubator. At predetermined time intervals, water was sampled and analyzed by UV−Vis spectroscopy at 300 nm. The concentration of released compounds was calculated by employing a calibration curve based on the crude CDs. The experiment was carried out in triplicate.

4.7. MB Photodegradation. A solution containing 5 ppm of MB and 2 g/L of GYI_{CDs} (Grain Yeast IPA purified CDs) or GYI_c (Grain Yeast IPA crude CDs) in MilliQ water was irradiated under UV light (365 nm, 80 Wm^{-2}) for 48 h. The absorbance at 665 nm was measured at predetermined time intervals, and the concentration of the residual MB was calculated by means of a calibration curve. The experiment was carried out in triplicate.

4.8. MB Absorption Test. To determine the MB absorption capability of the PVA-CD hydrogels, the sample (20 × 20 mm, 80 mg ca.) was soaked in a MB solution in MilliQ water (5 ppm). After 24 h of incubation, the hydrogel was removed, and the solution was analyzed by UV−Vis spectroscopy at 665 nm and its concentration was calculated by means of a calibration curve. The experiment was carried out in triplicate.

4.9. MB-PVA-CD Degradation. The MB-containing PVA-CD hydrogels were irradiated under UV light (365 nm, 80 Wm^{-2}) for 24 h. The degradation of the MB was qualitatively assessed visually.

■ ASSOCIATED CONTENT

Supporting Information

The Supporting Information is available free of charge at https://pubs.acs.org/doi/10.1021/acsomega.1c05403.

PL and PLE emission of the crude CDs (Figure S1); FT-IR of starting materials and crude CDs for Stout (a) and IPA (b) waste (Figure S2); DOSY-NMR spectra and data for crude CD samples (Figure S3 and Table S1); SEM micrographs (a,c) and laser diffraction profiles (b,d) of GYS CDs and GYI CDs (Figure S4); comparison of FT-IR spectra of crude and dialyzed CDs (Figure S5); degradation of the sole MB upon UV irradiation (control experiment) (a) and degradation rate of MB in the presence of SYS_c and SYS_{CDs} (b) (Figure S6); kinetics of release of fluorophores from PVA4 and PVA8 composite hydrogels (Figure S7); PL of PVA4 (a) and PVA8 (b) composites before and after the dialysis treatment (Figure S8); and photographs of PVA4 hydrogels after MB absorption, before and after 24 h of UV irradiation (cycles 1−5) (Figure S9) (PDF)

■ AUTHOR INFORMATION

Corresponding Authors

Matteo Gigli − *Department of Molecular Sciences and Nanosystems, Ca'Foscari University of Venice, 30172 Venezia Mestre, Italy; CSGI − Italian Research Center for Colloids and Surface Science, University of Florence, 50019 Firenze, Italy;* orcid.org/0000-0003-3899-0399; Email: matteo.gigli@unive.it

Claudia Crestini − *Department of Molecular Sciences and Nanosystems, Ca'Foscari University of Venice, 30172 Venezia Mestre, Italy; CSGI − Italian Research Center for Colloids and Surface Science, University of Florence, 50019 Firenze, Italy;* orcid.org/0000-0001-9903-2675; Email: claudia.crestini@unive.it

Authors

Simone Cailotto − *Department of Molecular Sciences and Nanosystems, Ca'Foscari University of Venice, 30172 Venezia Mestre, Italy; CSGI − Italian Research Center for Colloids and Surface Science, University of Florence, 50019 Firenze, Italy*

Daniele Massari − *Department of Molecular Sciences and Nanosystems, Ca'Foscari University of Venice, 30172 Venezia Mestre, Italy; CSGI − Italian Research Center for Colloids and Surface Science, University of Florence, 50019 Firenze, Italy*

https://doi.org/10.1021/acsomega.1c05403
ACS Omega 2022, 7, 4052−4061

Carlotta Campalani − *Department of Molecular Sciences and Nanosystems, Ca'Foscari University of Venice, 30172 Venezia Mestre, Italy;* orcid.org/0000-0001-9364-4718
Massimo Bonini − *CSGI − Italian Research Center for Colloids and Surface Science and Department of Chemistry "Ugo Schiff", University of Florence, 50019 Firenze, Italy;* orcid.org/0000-0002-9041-6047
Shujie You − *Division of Material Science, Department of Engineering Sciences and Mathematics, Luleå University of Technology, 97187 Luleå, Sweden;* orcid.org/0000-0001-7475-6394
Alberto Vomiero − *Department of Molecular Sciences and Nanosystems, Ca'Foscari University of Venice, 30172 Venezia Mestre, Italy; Division of Material Science, Department of Engineering Sciences and Mathematics, Luleå University of Technology, 97187 Luleå, Sweden*
Maurizio Selva − *Department of Molecular Sciences and Nanosystems, Ca'Foscari University of Venice, 30172 Venezia Mestre, Italy;* orcid.org/0000-0002-9986-2393
Alvise Perosa − *Department of Molecular Sciences and Nanosystems, Ca'Foscari University of Venice, 30172 Venezia Mestre, Italy;* orcid.org/0000-0003-4544-8709

Complete contact information is available at: https://pubs.acs.org/10.1021/acsomega.1c05403

Author Contributions

⊥S.C. and D.M. contributed equally.

Author Contributions

D.M.: investigation and validation; S.C.: investigation, validation, data curation, and writing original draft; M.G.: conceptualization, methodology, data curation, funding acquisition, writing original draft and review, and supervision; C.C.: kinetics of dye degradation; M.B.: laser diffraction analysis and SEM analysis; S.Y.: quantum yield and CD lifetime analysis; A.V., M.S., and A.P.: funding acquisition and review of the manuscript draft; C.C.: conceptualization, project administration, funding acquisition, and writing-review. All authors have given approval to the final version of the manuscript.

Funding

M.G. gratefully acknowledges Ca′ Foscari University FPI2019 grant. S.Y. and A.V. acknowledge the Kempe Foundation and the Knut & Alice Wallenberg Foundation for financial support.

Notes

The authors declare no competing financial interest.

REFERENCES

(1) Stahel, W. R. The Circular Economy. *Nat. News* **2016**, *531*, 435−438.
(2) Poliakoff, M.; Fitzpatrick, J. M.; Farren, T. R.; Anastas, P. T. Green Chemistry: Science and Politics of Change. *Science* **2002**, *297*, 807−810.
(3) Sheldon, R. A. Green Chemistry, Catalysis and Valorization of Waste Biomass. *J. Mol. Catal. A: Chem.* **2016**, *422*, 3−12.
(4) Briens, C.; Piskorz, J.; Berruti, F. Biomass Valorization for Fuel and Chemicals Production−A Review. *Int. J. Chem. React. Eng.* **2008**, *6*, 1674.
(5) Liguori, R.; Amore, A.; Faraco, V. Waste Valorization by Biotechnological Conversion into Added Value Products. *Appl. Microbiol. Biotechnol.* **2013**, *97*, 6129−6147.
(6) Rachwał, K.; Waśko, A.; Gustaw, K.; Polak-Berecka, M. Utilization of Brewery Wastes in Food Industry. *PeerJ* **2020**, *8*, No. e9427.
(7) Outeiriño, D.; Costa-Trigo, I.; Paz, A.; Deive, F. J.; Rodríguez, A.; Domínguez, J. M. Biorefining Brewery Spent Grain Polysaccharides through Biotuning of Ionic Liquids. *Carbohydr. Polym.* **2019**, *203*, 265−274.
(8) Pérez-Torrado, R.; Gamero, E.; Gómez-Pastor, R.; Garre, E.; Aranda, A.; Matallana, E. Yeast Biomass, an Optimised Product with Myriad Applications in the Food Industry. *Trends Food Sci. Technol.* **2015**, *46*, 167−175.
(9) dos Mathias, T. R. S.; Alexandre, V. M. F.; Cammarota, M. C.; de Mello, P. P. M.; Sérvulo, E. F. C. Characterization and Determination of Brewer's Solid Wastes Composition. *J. Inst. Brew.* **2015**, *121*, 400−404.
(10) Ferreira, I. M. P. L. V. O.; Pinho, O.; Vieira, E.; Tavarela, J. G. Brewer's Saccharomyces Yeast Biomass: Characteristics and Potential Applications. *Trends Food Sci. Technol.* **2010**, *21*, 77−84.
(11) Jacob, F. F.; Striegel, L.; Rychlik, M.; Hutzler, M.; Methner, F.-J. Spent Yeast from Brewing Processes: A Biodiverse Starting Material for Yeast Extract Production. *Fermentation* **2019**, *5*, 51.
(12) Pacheco, M. T. B.; Caballero-Córdoba, G. M.; Sgarbieri, V. C. Composition and Nutritive Value of Yeast Biomass and Yeast Protein Concentrates. *J. Nutr. Sci. Vitaminol.* **1997**, *43*, 601−612.
(13) Mussatto, S. I.; Dragone, G.; Roberto, I. C. Brewers' Spent Grain: Generation, Characteristics and Potential Applications. *J. Cereal Sci.* **2006**, *43*, 1−14.
(14) Puligundla, P.; Mok, C.; Park, S. Advances in the Valorization of Spent Brewer's Yeast. *Innovative Food Sci. Emerging Technol.* **2020**, *62*, No. 102350.
(15) Dabaro, M. D.; Demsash, H. D. Valorization of Agro-Industrial Waste into Bioethanol: A Case of Brewers Spent Grain. *Int. J. Renew. Energy Commer.* **2020**, *6*, 1−20.
(16) Comelli, R. N.; Seluy, L. G.; Benzzo, M. T.; Isla, M. A. Combined Utilization of Agro-Industrial Wastewaters for Non-Lignocellulosic Second-Generation Bioethanol Production. *Waste Biomass Valorization* **2020**, *11*, 265−275.
(17) Radosavljević, M.; Pejin, J.; Pribić, M.; Kocić-Tanackov, S.; Romanić, R.; Mladenović, D.; Djukić-Vuković, A.; Mojović, L. Utilization of Brewing and Malting By-Products as Carrier and Raw Materials in L-(+)-Lactic Acid Production and Feed Application. *Appl. Microbiol. Biotechnol.* **2019**, *103*, 3001−3013.
(18) Radosavljević, M.; Pejin, J.; Pribić, M.; Kocić-Tanackov, S.; Mladenović, D.; Djukić-Vuković, A.; Mojović, L. Brewing and Malting Technology By-Products as Raw Materials in L-(+)-Lactic Acid Fermentation. *J. Chem. Technol. Biotechnol.* **2020**, *95*, 339−347.
(19) Chen, K.-Q.; Li, J.; Ma, J.-F.; Jiang, M.; Wei, P.; Liu, Z.-M.; Ying, H.-J. Succinic Acid Production by Actinobacillus Succinogenes Using Hydrolysates of Spent Yeast Cells and Corn Fiber. *Bioresour. Technol.* **2011**, *102*, 1704−1708.
(20) Mohamad Ansor, N.; Abdullah, N.; Aminudin, N. Anti-Angiotensin Converting Enzyme (ACE) Proteins from Mycelia of Ganoderma Lucidum (Curtis) P. Karst. *BMC Complementary Altern. Med.* **2013**, *13*, 256.
(21) Low, K.-S.; Lee, C. K.; Low, C. H. Sorption of Chromium (VI) by Spent Grain under Batch Conditions. *J. Appl. Polym. Sci.* **2001**, *82*, 2128−2134.
(22) Li, Q.; Chai, L.; Qin, W. Cadmium(II) Adsorption on Esterified Spent Grain: Equilibrium Modeling and Possible Mechanisms. *Chem. Eng. J.* **2012**, *197*, 173−180.
(23) Low, K. S.; Lee, C. K.; Liew, S. C. Sorption of Cadmium and Lead from Aqueous Solutions by Spent Grain. *Process Biochem.* **2000**, *36*, 59−64.
(24) de Castro, K. C.; Cossolin, A. S.; dos Reis, H. C. O.; de Morais, E. B.; de Castro, K. C.; Cossolin, A. S.; dos Reis, H. C. O.; de Morais, E. B. Biosorption of Anionic Textile Dyes from Aqueous Solution by Yeast Slurry from Brewery. *Braz. Arch. Biol. Technol.* **2017**, *60*, No. e17160101.
(25) Kim, T.-Y.; Lee, J.-W.; Cho, S.-Y. Application of Residual Brewery Yeast for Adsorption Removal of Reactive Orange 16 from Aqueous Solution. *Adv. Powder Technol.* **2015**, *26*, 267−274.

(26) Robertson, J. A.; I'Anson, K. J. A.; Treimo, J.; Faulds, C. B.; Brocklehurst, T. F.; Eijsink, V. G. H.; Waldron, K. W. Profiling Brewers' Spent Grain for Composition and Microbial Ecology at the Site of Production. *LWT − Food Sci. Technol.* **2010**, *43*, 890−896.
(27) Tuerhong, M.; Xu, Y.; Yin, X.-B. Review on Carbon Dots and Their Applications. *Chin. J. Anal. Chem.* **2017**, *45*, 139−150.
(28) Liu, M. L.; Chen, B. B.; Li, C. M.; Huang, C. Z. Carbon Dots: Synthesis, Formation Mechanism, Fluorescence Origin and Sensing Applications. *Green Chem.* **2019**, *21*, 449−471.
(29) Xiao, L.; Sun, H. Novel Properties and Applications of Carbon Nanodots. *Nanoscale Horiz.* **2018**, *3*, 565−597.
(30) Mishra, V.; Patil, A.; Thakur, S.; Kesharwani, P. Carbon Dots: Emerging Theranostic Nanoarchitectures. *Drug Discovery Today* **2018**, *23*, 1219−1232.
(31) Yan, F.; Sun, Z.; Zhang, H.; Sun, X.; Jiang, Y.; Bai, Z. The Fluorescence Mechanism of Carbon Dots, and Methods for Tuning Their Emission Color: A Review. *Microchim. Acta* **2019**, *186*, 583.
(32) Amadio, E.; Cailotto, S.; Campalani, C.; Branzi, L.; Raviola, C.; Ravelli, D.; Cattaruzza, E.; Trave, E.; Benedetti, A.; Selva, M.; Perosa, A. Precursor-Dependent Photocatalytic Activity of Carbon Dots. *Molecules* **2020**, *25*, 101.
(33) Kang, C.; Huang, Y.; Yang, H.; Yan, X. F.; Chen, Z. P. A Review of Carbon Dots Produced from Biomass Wastes. *Nanomaterials* **2020**, *10*, 2316.
(34) Meng, W.; Bai, X.; Wang, B.; Liu, Z.; Lu, S.; Yang, B. Biomass-Derived Carbon Dots and Their Applications. *Energy Environ. Mater.* **2019**, *2*, 172−192.
(35) Campalani, C.; Cattaruzza, E.; Zorzi, S.; Vomiero, A.; You, S.; Matthews, L.; Capron, M.; Mondelli, C.; Selva, M.; Perosa, A. Biobased Carbon Dots: From Fish Scales to Photocatalysis. *Nanomaterials* **2021**, *11*, 524.
(36) Jin, S. H.; Kim, D. H.; Jun, G. H.; Hong, S. H.; Jeon, S. Tuning the Photoluminescence of Graphene Quantum Dots through the Charge Transfer Effect of Functional Groups. *ACS Nano* **2013**, *7*, 1239−1245.
(37) Zhu, S.; Zhang, J.; Tang, S.; Qiao, C.; Wang, L.; Wang, H.; Liu, X.; Li, B.; Li, Y.; Yu, W.; Wang, X.; Sun, H.; Yang, B. Surface Chemistry Routes to Modulate the Photoluminescence of Graphene Quantum Dots: From Fluorescence Mechanism to Up-Conversion Bioimaging Applications. *Adv. Funct. Mater.* **2012**, *22*, 4732−4740.
(38) Song, Y.; Zhu, S.; Zhang, S.; Fu, Y.; Wang, L.; Zhao, X.; Yang, B. Investigation from Chemical Structure to Photoluminescent Mechanism: A Type of Carbon Dots from the Pyrolysis of Citric Acid and an Amine. *J. Mater. Chem. C* **2015**, *3*, 5976−5984.
(39) Xiong, Y.; Schneider, J.; Ushakova, E. V.; Rogach, A. L. Influence of Molecular Fluorophores on the Research Field of Chemically Synthesized Carbon Dots. *Nano Today* **2018**, *23*, 124−139.
(40) Qu, D.; Sun, Z. The Formation Mechanism and Fluorophores of Carbon Dots Synthesized via a Bottom-up Route. *Mater. Chem. Front.* **2020**, *4*, 400−420.
(41) Essner, J. B.; Kist, J. A.; Polo-Parada, L.; Baker, G. A. Artifacts and Errors Associated with the Ubiquitous Presence of Fluorescent Impurities in Carbon Nanodots. *Chem. Mater.* **2018**, *30*, 1878−1887.
(42) Shi, L.; Hai Yang, J.; Bo Zeng, H.; Mei Chen, Y.; Chun Yang, S.; Wu, C.; Zeng, H.; Yoshihito, O.; Zhang, Q. Carbon Dots with High Fluorescence Quantum Yield: The Fluorescence Originates from Organic Fluorophores. *Nanoscale* **2016**, *8*, 14374−14378.
(43) Schneider, J.; Reckmeier, C. J.; Xiong, Y.; von Seckendorff, M.; Susha, A. S.; Kasák, P.; Rogach, A. L. Molecular Fluorescence in Citric Acid-Based Carbon Dots. *J. Phys. Chem. C* **2017**, *121*, 2014−2022.
(44) Mintz, K. J.; Zhou, Y.; Leblanc, R. M. Recent development of carbon quantum dots regarding their optical properties, photoluminescence mechanism, and core structure. *Nanoscale* **2019**, *11*, 4634−4652.
(45) Wang, C.; Strauss, V.; Kaner, R. B. Carbon Nanodots for Capacitor Electrodes. *Trends Chem.* **2019**, *1*, 858−868.
(46) Pirsaheb, M.; Mohammadi, S.; Salimi, A. Current Advances of Carbon Dots Based Biosensors for Tumor Marker Detection, Cancer Cells Analysis and Bioimaging. *TrAC, Trends Anal. Chem.* **2019**, *115*, 83−99.
(47) Gao, N.; Huang, L.; Li, T.; Song, J.; Hu, H.; Liu, Y.; Ramakrishna, S. Application of Carbon Dots in Dye-Sensitized Solar Cells: A Review. *J. Appl. Polym. Sci.* **2020**, *137*, 48443.
(48) Zhao, H.; Liu, G.; You, S.; Camargo, F. V. A.; Zavelani-Rossi, M.; Wang, X.; Sun, C.; Liu, B.; Zhang, Y.; Han, G.; Vomiero, A.; Gong, X. Gram-Scale Synthesis of Carbon Quantum Dots with a Large Stokes Shift for the Fabrication of Eco-Friendly and High-Efficiency Luminescent Solar Concentrators. *Energy Environ. Sci.* **2021**, *14*, 396−406.
(49) Cailotto, S.; Amadio, E.; Facchin, M.; Selva, M.; Pontoglio, E.; Rizzolio, F.; Riello, P.; Toffoli, G.; Benedetti, A.; Perosa, A. Carbon Dots from Sugars and Ascorbic Acid: Role of the Precursors on Morphology, Properties, Toxicity, and Drug Uptake. *ACS Med. Chem. Lett.* **2018**, *9*, 832−837.
(50) Cailotto, S.; Mazzaro, R.; Enrichi, F.; Vomiero, A.; Selva, M.; Cattaruzza, E.; Cristofori, D.; Amadio, E.; Perosa, A. Design of Carbon Dots for Metal-Free Photoredox Catalysis. *ACS Appl. Mater. Interfaces* **2018**, *10*, 40560−40567.
(51) Cailotto, S.; Negrato, M.; Daniele, S.; Luque, R.; Selva, M.; Amadio, E.; Perosa, A. Carbon Dots as Photocatalysts for Organic Synthesis: Metal-Free Methylene−Oxygen-Bond Photocleavage. *Green Chem.* **2020**, *22*, 1145−1149.
(52) Achilleos, D. S.; Yang, W.; Kasap, H.; Savateev, A.; Markushyna, Y.; Durrant, J. R.; Reisner, E. Solar Reforming of Biomass with Homogeneous Carbon Dots. *Angew. Chem., Int. Ed.* **2020**, *132*, 18341−18345.
(53) Bhati, A.; Anand, S. R.; Gunture; Garg, A. K.; Khare, P.; Sonkar, S. K. Sunlight-Induced Photocatalytic Degradation of Pollutant Dye by Highly Fluorescent Red-Emitting Mg-N-Embedded Carbon Dots. *ACS Sustainable Chem. Eng.* **2018**, *6*, 9246−9256.
(54) Hutton, M. G. A.; Martindale, B. C. M.; Reisner, E. Carbon Dots as Photosensitisers for Solar-Driven Catalysis. *Chem. Soc. Rev.* **2017**, *46*, 6111−6123.
(55) Zheng, C.; An, X.; Yin, T. New Metal-Free Catalytic Degradation Systems with Carbon Dots for Thymol Blue. *New J. Chem.* **2017**, *41*, 13365−13369.
(56) Rodrigues, C. V.; Correa, J. R.; Aiube, C. M.; Andrade, L. P.; Galvão, P. M.; Costa, P. A.; Campos, A. L.; Pereira, A. J.; Ghesti, G. F.; Felix, J. F.; Weber, I. T.; Neto, B. A.; Rodrigues, M. O. Down- and Up-Conversion Photoluminescence of Carbon-Dots from Brewing Industry Waste: Application in Live Cell-Imaging Experiments. *J. Braz. Chem. Soc.* **2015**, *26*, 2623−2628.
(57) Weiss, I. M.; Muth, C.; Drumm, R.; Kirchner, H. O. K. Thermal Decomposition of the Amino Acids Glycine, Cysteine, Aspartic Acid, Asparagine, Glutamic Acid, Glutamine, Arginine and Histidine. *BMC Biophys.* **2018**, *11*, 1−15.
(58) Prasannan, A.; Imae, T. One-Pot Synthesis of Fluorescent Carbon Dots from Orange Waste Peels. *Ind. Eng. Chem. Res.* **2013**, *52*, 15673−15678.
(59) Chen, C.-Y.; Tsai, Y.-H.; Chang, C.-W. Evaluation of the Dialysis Time Required for Carbon Dots by HPLC and the Properties of Carbon Dots after HPLC Fractionation. *New J. Chem.* **2019**, *43*, 6153−6159.
(60) Zhu, S.; Meng, Q.; Wang, L.; Zhang, J.; Song, Y.; Jin, H.; Zhang, K.; Sun, H.; Wang, H.; Yang, B. Highly Photoluminescent Carbon Dots for Multicolor Patterning, Sensors, and Bioimaging. *Angew. Chem., Int. Ed.* **2013**, *52*, 3953−3957.
(61) del Valle, J. C.; Catalán, J. Kasha's Rule: A Reappraisal. *Phys. Chem. Chem. Phys.* **2019**, *21*, 10061−10069.
(62) Liu, H.; Ding, L.; Chen, L.; Chen, Y.; Zhou, T.; Li, H.; Xu, Y.; Zhao, L.; Huang, N. A Facile, Green Synthesis of Biomass Carbon Dots Coupled with Molecularly Imprinted Polymers for Highly Selective Detection of Oxytetracycline. *J. Ind. Eng. Chem.* **2019**, *69*, 455−463.
(63) Wei, J.; Zhang, X.; Sheng, Y.; Shen, J.; Huang, P.; Guo, S.; Pan, J.; Feng, B. Dual Functional Carbon Dots Derived from Cornflour via

https://doi.org/10.1021/acsomega.1c05403
ACS Omega 2022, 7, 4052−4061

a Simple One-Pot Hydrothermal Route. *Mater. Lett.* **2014**, *123*, 107−111.
(64) Berrios, M.; Martín, M. Á.; Martín, A. Treatment of Pollutants in Wastewater: Adsorption of Methylene Blue onto Olive-Based Activated Carbon. *J. Ind. Eng. Chem.* **2012**, *18*, 780−784.
(65) Rani, U. A.; Ng, L. Y.; Ng, C. Y.; Mahmoudi, E.; Ng, Y.-S.; Mohammad, A. W. Sustainable Production of Nitrogen-Doped Carbon Quantum Dots for Photocatalytic Degradation of Methylene Blue and Malachite Green. *J. Water Process Eng.* **2020**, *40*, No. 101816.
(66) Peng, Z.; Zhou, Y.; Ji, C.; Pardo, J.; Mintz, K. J.; Pandey, R. R.; Chusuei, C. C.; Graham, R. M.; Yan, G.; Leblanc, R. M. Facile Synthesis of "Boron-Doped" Carbon Dots and Their Application in Visible-Light-Driven Photocatalytic Degradation of Organic Dyes. *Nanomaterials* **2020**, *10*, 1560.
(67) Jusuf, B. N.; Sambudi, N. S.; Isnaeni; Samsuri, S. Microwave-Assisted Synthesis of Carbon Dots from Eggshell Membrane Ashes by Using Sodium Hydroxide and Their Usage for Degradation of Methylene Blue. *J. Environ. Chem. Eng.* **2018**, *6*, 7426−7433.
(68) Galagan, Y.; Su, W.-F. Reversible Photoreduction of Methylene Blue in Acrylate Media Containing Benzyl Dimethyl Ketal. *J. Photochem. Photobiol. A* **2008**, *195*, 378−383.
(69) Younis, A.; Loucif, A. Defects mediated enhanced catalytic and humidity sensing performance in ceria nanorods. *Ceram. Int.* **2021**, *47*, 15500−15507.
(70) Sui, B.; Li, Y.; Yang, B. Nanocomposite hydrogels based on carbon dots and polymers. *Chin. Chem. Lett.* **2020**, *31*, 1443−1447.
(71) Shao, J.; Yu, Q.; Wang, S.; Hu, Y.; Guo, Z.; Kang, K.; Ji, X. Poly(Vinyl Alcohol)−Carbon Nanodots Fluorescent Hydrogel with Superior Mechanical Properties and Sensitive to Detection of Iron(III) Ions. *Macromol. Mater. Eng.* **2019**, *304*, No. 1900326.
(72) Kwan, N. H. M.; Leo, C. P.; Arosa Senanayake, S. M. N.; Lim, G. K.; Tan, M. K. Carbon-Dot Dispersal in PVA Thin Film for Food Colorant Sensing. *J. Environ. Chem. Eng.* **2020**, *8*, No. 103187.
(73) El-Shamy, A. G.; Zayied, H. S. S. New Polyvinyl Alcohol/Carbon Quantum Dots (PVA/CQDs) Nanocomposite Films: Structural, Optical and Catalysis Properties. *Synth. Met.* **2020**, *259*, No. 116218.
(74) Nayak, S.; Prasad, S. R.; Mandal, D.; Das, P. Carbon Dot Cross-Linked Polyvinylpyrrolidone Hybrid Hydrogel for Simultaneous Dye Adsorption, Photodegradation and Bacterial Elimination from Waste Water. *J. Hazard. Mater.* **2020**, *392*, No. 122287.
(75) Hu, M.; Gu, X.; Hu, Y.; Deng, Y.; Wang, C. PVA/Carbon Dot Nanocomposite Hydrogels for Simple Introduction of Ag Nanoparticles with Enhanced Antibacterial Activity. *Macromol. Mater. Eng.* **2016**, *301*, 1352−1362.
(76) Singh, S.; Shauloff, N.; Jelinek, R. Solar-Enabled Water Remediation via Recyclable Carbon Dot/Hydrogel Composites. *ACS Sustainable Chem. Eng.* **2019**, *7*, 13186−13194.

https://doi.org/10.1021/acsomega.1c05403
ACS Omega 2022, 7, 4052−4061